Accepted Manuscript

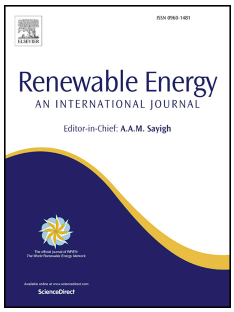

Efficiency and heat transfer improvements in a parabolic trough solar collector using TiO_2 nanofluids under turbulent flow regime

J. Subramani, P.K. Nagarajan, Omid Mahian, Ravishankar Sathyamurthy

PII: S0960-1481(17)31180-1

DOI: 10.1016/j.renene.2017.11.079

Reference: RENE 9481

To appear in: *Renewable Energy*

Received Date: 23 May 2017

Revised Date: 23 November 2017

Accepted Date: 25 November 2017

Please cite this article as: Subramani J, Nagarajan PK, Mahian O, Sathyamurthy R, Efficiency and heat transfer improvements in a parabolic trough solar collector using TiO_2 nanofluids under turbulent flow regime, *Renewable Energy* (2017), doi: 10.1016/j.renene.2017.11.079.

Efficiency and heat transfer improvements in a parabolic trough solar collector using TiO_2 nanofluids under turbulent flow regime

J.Subramani[a], P.K.Nagarajan[a]*, Omid Mahian[b], Ravishankar Sathyamurthy[a]

[a]Department of Mechanical Engineering, S.A.Engineering College, Chennai, Tamil Nadu,Affiliated to Anna University, India. Pin-600 077

[b]Department of Mechanical Engineering, Engineering Faculty, Ferdowsi University of Mashhad, Mashhad, Iran

** Corresponding author. Tel.:+91-9789815744; Fax: +91-44-26801899*

E-mail: pknagarajan@saec.ac.in, krishnaga77@gmail.com

ABSTRACT:

The efficiency of a parabolic trough solar collector (PTSC) was enhanced by using TiO_2/DI-H_2O (De-Ionized water) nanofluid. Test samples consisting of nanofluids with concentrations of 0.05%, 0.1%, 0.2%, and 0.5% were compared with deionized water (the base fluid) at different flow rates under turbulent flow regimes ($2950 \leq Re \leq 8142$). All the experiments were conducted to meet ASHRAE 93(2010) standards. Heat transfer and the flow characteristics of nanofluids through the collector were studied, and empirical correlations were developed in terms of the Nusselt number, friction factor, and performance index. The convective heat transfer coefficient was improved up to 22.76% by using TiO_2 nanofluids instead of the base fluid. It was found that TiO_2 nanofluid with a volume concentration of 0.2% (at a mass flow rate of 0.0667 kg/s) can provide the maximum efficiency enhancement in the PTSC (8.66% higher than the water-based collector). Consequently, the absorbed energy parameter was found to be 9.5% greater than that of the base fluid.

- *Keywords: Parabolic trough collector, nanofluid, titanium oxide, collector efficiency.*

1. Introduction

Nowadays, researchers are seeking clean energy sources as alternatives to fossil fuels. One of these sources is solar energy. Solar energy is abundant and could be used as a potential resource to meet global energy demands. According to the International Energy Agency (IEA) roadmap, the demand for concentrated solar energy will be about 1000 GW by the end of 2050 [1]. Using solar trough collectors is one of the methods to produce power from solar energy. Many studies have been done on the performance of solar trough collectors. For example, Bakos and Tsechelidou [2] have conducted an analysis of solar trough collectors using TRNSYS simulation software. They calculated plant efficiency, variations in power production, fuel usage, and emissions. Similarly, Borunda *et al.* [3] coupled a parabolic trough collector with a Rankine cycle and a co-generator for textile industries at medium temperatures. This analysis was performed by using TRNSYS. They observed an enhancement in thermal and electrical efficiency and showed the overall enhancement of global efficiency of the plant as a result of waste heat recovery. Furthermore, Karathanassis *et al.* [4] experimentally evaluated the performance of a concentrating parabolic thermal/photovoltaic (CPVT) system equipped with heat sinks to enhance cooling of the PV panels. The extent of improvement in electrical efficiency and thermal efficiency were 6% and 44%, respectively.

To optimize the collector performance, studies were conducted on the design aspects of parabolic trough solar collectors (PTSCs) and their geometrical parameters, such as the aperture area, rim angle, focal length, absorber diameter, concentration ratio, and other important optical parameters (such as reflectivity, receiver tube intercept factor, and incident angle) [5-8]. Realizing the importance of these variables, improvement in heat transfer capacity of working fluid was primarily developed by Xuan and Li [9], by implementing nanoparticles in the working

fluid for effective convective heat transfer. Subsequently, many investigators have used metal oxide-based nanoparticles (TiO_2,,Al_2O_3,CuO) blended with water for various heat transfer enhancement applications using the constant heat flux method. Table 1 provides a summary of some of these studies [10-15].

Nanofluid applications have been explored in various types of solar collectors. For instance, Tyagi *et al.* [16] observed that the addition of Al_2O_3 nanoparticles enhances the solar absorption rate by nine times that of pure water. This result suggests that the use of Al_2O_3 nanofluid enhances the efficiency of the system by 10%. Saidur *et al.*[17] experimentally investigated the thermal performance of Al_2O_3/H_2O as the working fluid on the direct solar absorption system. The result showed that the increase in volume fraction of Al_2O_3 up to 1% in the fluid enhanced the collector performance and absorption rate. Taylor *et al.* [18] studied the effect of graphite nanoparticles on the performance of high-flux concentrators. The result shows, a 10% enhancement of the thermal performance of the solar reflective dish collector caused by graphite nanoparticles. Otanicer *et al.* [19] investigated the effect of various nanofluids (graphite, CNT, silver nanoparticles) on the performance of the direct absorption solar collector (DASC). The results indicated that the use of nanofluids improved the efficiency of the (DASC) by 5%. He *et al.*[20] examined the light-to-heat swap performance of CNT/water and TiO_2/water in a vacuum tube solar collector and observed a higher efficiency for CNT/H_2O as compared to TiO_2 nanofluids. Yousefi *et al.* [21] studied the effect of Al_2O_3/H_2O nanofluids on the performance of a flat plate solar collector. The result revealed that nanofluids with 0.2% volume concentration increased the collector efficiency by 28%. Mahian *et al.* [22] studied the effects of Nusselt number and the thermal effects of four different nanofluids (CuO/H_2O, Al_2O_3/H_2O, TiO_2/H_2O, and SiO_2/H_2O) on the mini-channel based solar collector. Nanofluid based solar collectors have

been coupled to enhance the performance of other solar energy devices such as solar stills. For example, Mahian *et al.*[23] coupled two flat plate solar collectors for enhancing the productivity of a solar still equipped with a heat exchanger. A few classical reviews (Mahian *et al.* [24], Nagarajan *et al.*[25], and Bozorgan *et al.*[26]) have extensively explored the effects of nanofluids on the thermal performance of solar collectors.

The use of nanofluids in a solar PTC makes a significant improvement in thermal performance. For instance, a 5% volume concentration of Al_2O_3 nanoparticles in synthetic oil enhanced the average heat transfer coefficient of a solar PTC by 6% at a temperature of 500K [27]. For a 0.05% volume fraction, the deformation of the receiver tube caused a decrease from 2.1 mm to 0.59 mm, and the nanofluids reduced the temperature gradient and absorber surface temperature, which increased heat transfer by 1.2% at a velocity of 1m/s [28]. Khullar *et al.* [29] studied the performance of concentrated solar parabolic trough collector quantitatively and theoretically. The result showed that the efficiency of the solar collector could be enhanced using nanofluids in low concentrations by 5–10%. An investigation of solar PTCs using Syltherm800 and Al_2O_3 nanoparticles was done, and it was found that the efficiency of the PTC increases by 7.6% [30]. With concentrations of 0.2% and 0.3% multi-walled CNTs in mineral oil in a solar PTC, the thermal efficiency rise was about 4–7% [31]. Kaloudis *et al.* [32] studied the thermal performance of a solar trough collector using ANSYS-CFX software where the nanofluid contained Al_2O_3 nanoparticles with volume concentrations up to 4% where the base fluid was Syltherm800 oil. These results showed an improvement of about 10% in the collector efficiency with 4% volume concentration of Al_2O_3 nanoparticles. Bellos *et al.* [33] investigated the trough collector utilizing a converging-diverging receiver tube with a dimple sinusoidal wave profile for Thermal-oil/Al_2O_3 nanofluids. It was concluded that changes in the nanofluid concentrations

raised the efficiency by 4.25%. Similarly, changes in geometry as a parameter enhanced the efficiency of the collector by 4.55%. Elima-Ard *et al.*[34] investigated the heat transfer characteristics of a plain tube double twisted-tape with variations in the concentration of TiO_2 nanofluid. It was noticed that the increased concentration of TiO_2 nanoparticles, increases the heat transfer capacity by 9.9% to 11.2%. Furthermore, the overall thermal performance improved by 1.7–2.4%. Abdolbaqi *et al.* [35] studied the effects of heat transfer characteristics using bio glycol/water-based TiO_2 nanofluids in a 2% volume concentration in a flat-tube flow geometry. The thermal conductivity, viscosity, Nusselt number, and friction factor were enhanced by 12.6%, 20.5%, 28.2%, and 14.3%, respectively.

Menbari *et al.* [36] investigated the working of a direct absorption solar collector using the natural convective heat transfer method (transient heat flux method), and CuO/H_2O nanofluid. Uddin and Harmand [37] studied the transient operating condition of various nanofluids and concluded that TiO_2/H_2O provides a better natural convective heat transfer than CuO and Al_2O_3 nanofluids. Considering the characteristics of TiO_2 nanofluid, there is need for a study on the performance and heat transfer effects of PTSC using transient heat flux method. The study by Arani *et al*. [13] revealed that a TiO_2/H_2O nanofluid with a 20-nm particle size diameter yielding optimal results with particle size varied from 10–50 nm range.

Hence, the present work focuses on the PTSC thermal performance and heat transfer characteristics with a transient heat flux method using TiO_2 nanofluids. Another key goal of this investigation is to determine the maximum possible amount of heat energy from a stationary concentrating collector using low-volume concentration of TiO_2 nanofluid, as well as to estimate the efficiency and heat transfer characteristics of the PTSC. Based on the experimental

outcomes, empirical correlations for the Nusselt number, friction factor, and performance index are developed using multiple linear regression models.

2. Experimental methods and instrumentation

The design parameters for a solar PTC are the aperture, rim angle, acceptance angle, focus, depth, arc length, and receiver tube diameter, which were determined using the equations proposed by Kalogirou [38]. The mathematical model was simulated using the TracePro software package for reflectivity, absorptivity, and transmissivity above 0.9. The solar PTC design was mathematically verified by Duffie [39]. The experimental setup was located in Chennai, India (latitude 13^{o} 02’ 33” N and longitude 80^{o} 06’ 03” E) as shown in Fig.1–2.

The collector was made of an anodized aluminum reflector sheet with a mean measured reflectance value of 0.94. The receiver tube was a 2m copper tube with inner/outer diameters of 13 and 16 mm, respectively. The receiver tube was surrounded by a transparent borosilicate glass tube with a 30mm internal diameter and 34mm external diameter. The arrangement was sealed by a high temperature resistant cork for maintaining a partial vacuum for reducing convective heat losses and harnessing the incident solar energy by the greenhouse effect.

Carbon black powder up to 1 µm in thickness was coated over the external surface area of the absorber tube. The outer surface temperature was measured with WIKA TC50, and the thermo couples were placed at lengths of 20, 50, 90, 120, and 160 cm apart. The gradient pressure across the test rig was measured using an M5100 piezoelectric pressure transducer with an accuracy of ±1% and a range of 0-3.5bar. The TiO_2 nanofluid was stored in a reservoir and circulated to the entrance of the absorber tube by a centrifugal pump, which was operated by a rotameter with a range of 0–10 lpm and accuracy of ±1%. The absorber tube outlet was connected to a heat

exchanger for diminishing the temperature of the nanofluids. While the heat exchanger reduced the temperature by up to 3°C, a constant temperature bath was employed to balance the nanofluid temperature in accordance with the specifications of the ASHRAE 93(2010) [40] standards. The trough collector was always situated perpendicular to the solar noon, and the thermal performance of the non-tracking method (stationary) was studied according to the ASHRAE standards. The test parameters were also recorded based on these standards, including the ambient temperature, flow rate, wind velocity, solar radiation, temperatures at the entry and outlet of the test section, and gradient pressure. A pyranometer (SP Lite2 silicon) was used for the determination of direct solar radiation, while the wind velocity and ambient temperatures were measured using a vane-type anemometer with a range of 0–25 m/s and accuracy of ±3%. The solar collector test facility was designed and mounted for the outside ambient conditions with a mean wind speed of 5 m/s with an operating humidity range of 60–80%. The support structure was designed to resist a maximum wind speed of about 40 m/s. Detailed specifications of the PTSC are shown in Table 2.

3. Nanofluid preparation and characterization

The nanofluid was prepared from TiO_2 powder with 99.7% purity, an average size of 20 nm, a pH of 7, and a density of 4170 kg/m^3. The TiO_2 nanoparticles were obtained from Alfa Aesar, UK. The nanofluids were prepared with nanoparticle volume percentages of 0.05%, 0.1%, 0.2%, and 0.5%. The nanoparticles were dispersed in DI water by ultra-sonication to prevent agglomeration and ensure a pH value of 7. The zeta potential stability test was carried out for each concentration as shown in Table 3.

The TiO_2 nanoparticles were filtered using a mesh size of 0.5 µm and then dried in ambient air. The nanoparticles were characterized by SEM and EDAX as shown in Fig.3–4. The SEM

analysis was carried out on a CARL ZEISS SUPRA 55 scanning electron microscope. The theoretical and experimental thermo-physical properties of the nanofluids are compared in Table 4. The peaks for Ti and O for the EDAX results confirmed that the particles wereTiO_2. The theoretical thermo-physical properties of the TiO_2 nanofluids are shown in Table 5.

4. ASHRAE standards, testing methods, and data collection

In order to avoid the influence of weather ambiguity, ASHRAE [40] has established specific test methods for outdoor conditions using a stationary concentrating collector model. The investigations were carried out based on the ASHRAE test procedure. The irradiance of the direct beam should have been greater than 800 W/m^2, and the maximum radiation with a clear sky should have been 32 W/m^2 at a time interval of 10 minutes each. The wind velocity should have been between 2 and 4 m/s with a natural wind flow, and the heat transfer fluid flow rate should have been 0.02 kg/sm^2.

The performance analysis was conducted using two different methods, and the readings considered for the calculation were based on the time period around solar noon (9:00AM to 16:00PM). Testing was done with different fluid concentrations and flow rates in the receiver tube. The experiments were conducted by dividing the test cycles into six parts consisting of 60 minutes each. Every 60-minute cycle was further divided into 15minute sub-cycles to achieve steady-state conditions and to obtain a collector time constant of 63.2% to conform to the ASHRAE [40] standards. To implement the steady-state model, a minimum of 16 data points were obtained at various inlet fluid temperatures, and were used to identify the collector efficiency of the PTSC by linear regression. Data were collected daily for several months.

4.1 Time constant and incidence angle modifier (IAM)

The time constant reflects the heating capacity of a solar collector and is used for predicting its transient characteristics. The time constant is the time required for the fluid to achieve 63.2% of the steady-state value intransient operation conditions after a sudden change in the incident solar radiation. The collector time constant is determined using Eq. (5):

$$\left(T^{o} - T^{i}\right) = 0.632\left(T^{fo,ss} - T^{i}\right) \quad (5)$$

where $T^{fo,ss}$is steady-state working fluid outlet temperature (°C). The time constant (τ_o) obtained in the present study was 600sec for water and 273 sec for the 0.2% TiO_2 nanofluid at a mass flow rate of 0.0667kg/s (Fig.5a). These values show that the attainment of the steady-state was nearly 58% faster when using the nanofluids, because of the high absorptivity of the TiO_2 nanoparticles. Generally, the base fluid absorptivity is higher at a longer wavelength and that of the nanoparticles higher at a shorter wavelength. This allows the nanofluids to absorb radiation easily and attain steady-state conditions faster than water [45]. Fig.5b shows a plot of the incidence angle and IAM. IAM was determined by dividing the collector efficiency at a particular incidence angle (θ) and this is given in the ASHRAE standards. A third-order polynomial curve was obtained by linear fitting using Eq.(6):

$$K_{\alpha\tau} = 0.000000758\,\theta^3 - 0.000150\,\theta^2 - 0.00289\,\theta + 0.984 \quad (6)$$

4.2 Evaluation of collector efficiency

The collector efficiency depicts the useful heat gain in relation to the whole incident radiation received by the collector aperture area, which is given by Eq.(7–9).The useful heat gain of a TiO_2 nanofluid was calculated by [38]:

$$Q_g = mC_{p_{nf}}\left(T^{o} - T^{i}\right) \quad (7)$$

The collector efficiency of the solar PTC can be obtained by equations [38][39]:

$$\eta_c = \frac{Q_g}{A_a I} = \frac{mC_{p_{nf}}(T^o - T^i)}{A_a I} \quad (8)$$

The resultant curve of the collector efficiency was a series of 16 data points. The slope and intercept were found using a linear regression fit method. The efficiency of the collector was determined by equations [46]:

$$\eta_c = F_R(\tau\alpha) - \frac{F_R U_L}{C}\left(\frac{(T^o - T^a)}{I}\right) \quad (9)$$

Where $F_R(\eta_o) = F_R(\tau\alpha)$ is the absorbed energy parameter (intercept),

$\frac{F_R U_L}{C}$ is the removal energy parameter (slope),C is the concentration ratio, and

$\left(\frac{(T^o - T^a)}{I}\right)$ is the heat loss parameter or characteristic curve of the collector.

Fig.6 shows the relationship between the collector efficiency and the heat loss parameter. The values were computed using the current model and compared with previous models. The intercept factor $F_R(U_L)$ and slope factor $F_R(\tau\alpha)$ were obtained using a linear regression fit method. The maximum collector efficiency for TiO_2 with 0.2% volume concentration was 57%, which was 8.66% more than that of the base fluid (DI) water for a similar flow rate. The regression equation for the collector efficiency with DI water and the TiO_2 nanofluids are shown in Table 6.

The significant values for the PTC parameters are shown in Table 7.The experimental results reveal that at a lower mass flow rate (m=0.0083 kg/s), the maximum outlet temperature(T=93.15°C) was a result of the higher contact time between the receiver surface and

the working fluid. Furthermore, at the maximum flow rate (m=0.0667 kg/s), the temperature gradient $\Delta T= (T^w-T^b)$ was lower, which resulted in a higher convective heat transfer coefficient.

4.3. Data reduction

The Reynolds number, Nusselt number, friction factor, convective heat transfer coefficient, and solar collector efficiency were the five important factors in the solar PTC parametric values that could be calculated using the test results. The equations used are shown in Table 8.

4.4. Uncertainty analysis

An approach described by Coleman and Steele [50] was applied to estimate the uncertainties in the results. All the experimental values were averaged for the calculations and regression methods. The uncertainties were found in the experimental measurement of the independent variables (T,Q_g, and I) as a result of variable outcomes that were determined from the derived variables (Nu, Re, f, and η_c). The standard deviation was manipulated from the derived uncertainty, which was calculated by repeating each variable for at least three intervals.

$$\epsilon_R = \left[\left(\frac{\epsilon_1 \partial R}{\partial X_1}\right)^2 + \left(\frac{\epsilon_2 \partial R}{\partial X_2}\right)^2 + \left(\frac{\epsilon_3 \partial R}{\partial X_3}\right)^2 + \cdots\cdots + \left(\frac{\epsilon_n \partial R}{\partial X_n}\right)^2\right]^{0.5} \quad (19)$$

The relative error can be calculated as follows:

$$\dot{E}_R = \epsilon_R/R\ \% \quad (20)$$

The efficiency of the solar PTC directly depends on the mass flow rate, fluid inlet temperature, outlet temperature, and direct normal irradiance (T^i, T^o, Q_g, and I). The uncertainty of the efficiency of solar collector is given by the subsequent equation:

$$\eta_c = f\left(Q_g,\ T^i, T^o, I\right) \quad (21)$$

$$\epsilon_{\eta c} = \sqrt{\left[\left(\frac{\partial \eta c}{\partial Q_g}\right)^2 \left(\epsilon_{Q_g}\right)^2 + \left(\frac{\partial \eta c}{\partial T^i}\right)^2 (\epsilon T^i)^2 + \left(\frac{\partial \eta c}{\partial T^o}\right)^2 (\epsilon T^o)^2 + \left(\frac{\partial \eta c}{\partial I}\right)^2 (\epsilon_I)^2\right]} \quad (22)$$

Velocity is a function of flow rate (m):	$\left(\epsilon_{u_m}\right) = \sqrt{\left[\left(\frac{\partial u_m}{\partial m}\right)^2 \epsilon_m{}^2\right]}$ - Eq.(23)
Reynolds number (Re) is a function of velocity (u_m):	$\left(\epsilon_{Re}\right) = \sqrt{\left[\left(\frac{\partial Re}{\partial u_m}\right)^2 \epsilon_{u_m}{}^2\right]}$ - Eq.(24)
The Nusselt number (Nu) is a function of the Re:	$\left(\epsilon_{Nu}\right) = \sqrt{\left[\left(\frac{\partial Nu}{\partial Re}\right)^2 \epsilon_{Re}{}^2\right]}$ - Eq.(25)
The friction factor (f) is a function of the pressure drop (ΔP):	$\left(\epsilon_f\right) = \sqrt{\left[\left(\frac{\partial f}{\partial \Delta P}\right)^2 \epsilon_{\Delta P}{}^2\right]}$ - Eq.(26)

The uncertainty error percentage values are shown in Table 9. The maximum deviations in the uncertainty were3.65%, 3.21%, 4.58%, and 2.96% for the Reynolds number, Nusselt number, friction factor, and collector efficiency, respectively.

5. Results and discussion

Fig.7a shows the absorbed energy factor $F_R(\tau\alpha)$ for varied concentrations of nanoparticles at different flow rates. A peak value of 0.5761 was obtained, which was 9.5% greater than that of the base fluid. The enhancement in the absorbed energy factor was achieved by an addition of nanoparticles, because it is a function of the nanofluids velocity, thermal conductivity, and specific heat capacity of the working fluid. Although the nanoparticles caused an increase in the

heat absorption rate, this yielded only an optimal result at a 0.2% volume concentration because of the fact that "as the viscosity increased, the flow rate decreased." This, in turn, reduced the Reynolds number. As a result, the heat transfer coefficient declined and subsequently lowered the Nusselt number. Thus, a lower concentration was used for avoiding a reduction in the absorbed energy factor. As shown in Fig.7b, the removal energy factor, $F_R(U_L)$, for concentrations and flow rates was considered to pass in the range of 6.4–8.5. The overall collector heat loss coefficient (U_L) was 8.845–9.042 W/m^{2}K, and the average removal energy factor of the collector $F_R(U_L)$ was 7.48. Hence, the flow rate changed the internal heat transfer coefficient, but the (U_L) was almost constant around 8.86 W/m^{2}K. Therefore, the overall collector heat loss coefficient (U_L) was roughly constant upon variations in the flow rates regardless of the nanoparticle concentration. The removal energy factor, $F_R(U_L)$,deviated moderately as a result of the pH value of nanofluids [51].

Fig.8(a–c) shows the characteristic curves of the PTSC for three different flow rates: 0.0083, 0.0333, and 0.0667 kg/s. The efficiency is plotted against the heat loss parameter, $(T^i-T^a)/I$, for each of the flow rates. Among the various flow rates and concentrations, a maximum collector efficiency of 56.86% was obtained at 0.0667kg/s at 0.2% volume concentration as shown in Fig.8c. This result shows that there was an 8.66% increase in collector efficiency and 22.76% rise in convective heat transfer compared to that of water. Such an increase in collector efficiency and convective heat transfer was due to an increase in the absorptivity and absorption coefficient of the nanoparticles. Consequently, this increased the convective heat transfer coefficient of the nanofluid as a result of the reduction in the gradient temperature, $\Delta T=(T^w-T^b)$. It was also observed that an average overall collector heat loss coefficient (U_L) of 8.86 W/m^{2}K was achieved for each of the varying flow rates and concentrations. Further increases in the

volume concentration from 0.2% to 0.5% resulted in an enhancement in solar PTC efficiency of only 9.36% compared to that of water. This result clearly showed an incremental addition in the collector efficiency as only 0.6% for the increased volume concentration of 0.5% for the varying flow rates as shown in Fig.8d. Since the average improvement in solar PTC efficiency was <1% at a 0.5% volume concentration, the optimal volume concentration could be limited to 0.2%. In addition, the flow rate was seen as inversely proportional to the gradient temperature. As a result, a rise in flow rate caused improvement in heat transfer coefficient and a decrease in the gradient temperature (ΔT), leading to increased collector efficiency.

Fig.9 (a–b) shows plots of the temperature gradient for different flow rates and nanoparticle concentrations, as well as the convective heat transfer coefficients for different flow rates. From these two graphs, we can clearly correlate the flow rate, temperature gradient, and convective heat transfer coefficient. For higher flow rates, the temperature gradient was low and the heat transfer coefficient was higher. At lower flow rates, the temperature gradient was higher and the heat transfer coefficient was lower because the surface contact time (flow through time) was more in comparison to the higher flow rates. When using nanofluids, it was possible to achieve a temperature gradient of 16.24°C at lower mass flow rates and 3.877°C at higher mass flow rates, which resulted in a reduction of 35.88% when compared to water.

Plots for the experimental and predicated Nusselt numbers at dissimilar flow rates and concentrations are shown in Fig.10(a–b). The error between the predicted value and experimental value was around ±5.8%. The empirical correlation equation for different Nusselt numbers and Reynolds numbers were based on dissimilar flow rates and volume concentrations, which was given in Eq. (27). The correlation was compared to data from previous studies in Fig. 10. The present model was developed for the Reynolds number range of ($2950 \leq Re \leq 8142$) and the

Prandtl number range of (5.78 to 4.65) with a collector efficiency of around 57%. The results were compared to those of the Mweswigye model [30], which predicted the Nusselt number with 10% accuracy for the Reynolds number range of ($3560 \leq Re \leq 1.15x10^5$) and particle concentrations of $0 \leq \phi \leq 8\%$. Despite variations as a result of design parameters, testing methods, and fluid properties, the results agree well with those of the previous models.

Plots of the experimental and predicted friction factors are given in Fig.11(a–b) for different flow rates and concentrations. The friction factor was estimated as a function of the pressure drop and roughness fraction of the absorber tube, which was negligible. Consequently, the average pressure drop in the solar PTC system was measured as 1.46 kPa. The present model showed a deviation of about ±3.4% from the measured friction factor. It was evaluated using the results of the Mweswigye model [30], and the predicted friction factor showed ±8% accuracy for a higher Reynolds number. Fig.12a depicts the experimental and predicted performance indices for different flow rates and nanoparticle concentrations with a deviation of around ±6.9%. Fig.12b shows the variations in the performance index for different Reynolds numbers and nanoparticle concentrations. The highest performance index of 1.39 occurred at a 0.2% volume concentration and a mass flow rate of 0.0667 kg/s. The performance index of the TiO_2 nanofluid was greater than 1, implying that it would enhance the heat transfer in a solar PTC application.

Variations in the performance index are based on variations in the pH and thermo-physical properties of the nanofluids. The particle size also influences the performance of the solar PTC. Nanoparticles with larger sizes that tend to scatter radiation rather than absorb it. Hence, it is recommended that the dimension of the nanoparticles be <50 nm to have an effective heat transfer. In the present study, the TiO_2 nanoparticles had an average size of 20 nm. Hence, the heat transfer was enhanced and the nanoparticles were found suitable for solar PTC applications.

The following are the empirical correlations for the Nusselt number, friction factor, and performance index for TiO_2water nanofluids in the flow range of (2950≤Re≤8142) in a solar PTC receiver tube:

$$\mathrm{Nu_c} = 0.02169\, Re^{0.836} Pr^{0.071} (1 + \phi)^{0.30} \quad (27)$$

$$f_c = 0.46673\, Re^{-0.349} Pr^{0.246} (1 + \phi)^{0.204} \quad (28)$$

$$P_{indexc} = 0.69628\, Re^{0.0399} (1 + \phi)^{1.387} \quad (29)$$

6. Conclusions

This study investigated the performance of the TiO_2 nanofluid to document its heat transfer capability for solar PTC applications. Tests were conducted using different nanoparticle concentrations and mass flow rates, and the following outcomes were obtained:

1. Nanofluids have a 9.5% higher absorbed energy factor $F_R(\tau\alpha)$ compared to water.
2. At ϕ=0.2% and a mass flow rate of 0.0667 kg/s, the absorbed energy factor $F_R(\tau\alpha)$has a higher value, while the removal energy factor $F_R(U_L)$ value fluctuates marginally.
3. A higher convective heat transfer coefficient is achieved at a maximum flow rate of 0.0667kg/s because of the lower temperature gradient (ΔT=3.89°C). The overall collector heat loss coefficient (U_L) does not deviate significantly from 8.86 W/m^{2}K despite variations in flow rates and concentrations.
4. Correlations show that the Nusselt number, friction factor, and performance index are in the Reynolds number range of (2950≤Re≤8142).
5. The performance index has a peak value of 1.39 for the nanofluid with a volume concentration of 0.2% and a mass flow rate of 0.0667 kg/s.
6. The maximum overall efficiency of the PTSC using TiO_2 nanofluid is 57%, which is 9% greater than that of the base fluid.

7. The empirical correlations for the heat transfer characteristics are as follows:

$$\mathrm{Nu_c} = 0.02169\, Re^{0.836} Pr^{0.071} (1 + \phi)^{0.30}$$

$$f_c = 0.46673\, Re^{-0.349} Pr^{0.246} (1 + \phi)^{0.204}$$

$$P_{indexc} = 0.69628\, Re^{0.0399} (1 + \phi)^{1.387}$$

The above correlations are valid for volume concentrations up to 0.2% and Reynolds numbers between 2950 and 8142 in which the working fluid is a TiO_2/water nanofluid.

Acknowledgements

The authors thankfully acknowledge the financial support provided by the (No.SB/FTP/ETA-444/2012)Science and Engineering Research Board (SERB), DST, India.

Nomenclature

A_a –Ccollector aperture area (m^2)

C_p – Specific heat capacity (kJ/kg K)

d_i – Receiver tube inner diameter, m

d_o – Receiver tube outer diameter, m

f – Friction factor

h – Convective heat transfer coefficient (W/m^2 K)

I– Direct normal irradiance, W/m^2

k – Thermal conductivity, W/m K

$K_{\alpha\tau}$– Incidence angle modifier

L - Length of the receiver tube, m

m – Mass flow rate (kg/s)

Nu – Nusselt number

Pr – Prandtl number

P_{index} – Performance index

ΔP- Pressure drop of the fluid in (kPa)

Q_g – Useful heat gain (W)

Re – Reynolds number

T^a – Ambient temperature (^oC)

T^i – Inlet temperature of the working fluid (^oC)

T^o – Outlet temperature of the working fluid (^oC)

$T^{fo,ss}$ - Steady state working fluid outlet temperature (^oC)

T^w – Mean wall temperature (^oC)

T^b – Bulk mean temperature (^oC)

$\Delta T=(T^w-T^b)$ - Gradient temperature of nanofluid, (^oC)

u –working fluid velocity, (m/s)

395 $F_R(\eta_o) = F_R(\tau\alpha)$ - Absorbed energy parameter (intercept)

396 $\frac{F_R U_L}{C}$ - Removal energy parameter (slope) and C - Concentration ratio

397 $\left(\frac{(T^o - T^a)}{I}\right)$: Heat loss parameter or characteristic curve of the collector

398 ASHRAE–American Society of Heating, Refrigeration and Air-conditioning Engineers

399 PTC – Parabolic Trough Collector

400 PTSC – Parabolic Trough Solar Collector

401 SFPC – Solar Flat Plate Collector

402 SSA – Specific Surface Area

403 IAM – Incident Angle Modifier

404 DI – De-ionized water

405 *Greek Symbols*

406 α – fluid thermal diffusivity (m^2/s)

407 μ – Dynamic viscosity, Ns/m^2

408 ρ – Density, Kg/m^2

409 ϕ_r– Rim angle (degrees)

410 ϕ – Nanoparticles volume concentration, %

411 θ- Angle of incidence, degrees

412 η_c – Collector efficiency

413 τ_o – Time constant, sec

Subscripts

bf – base fluid

nf – nanofluid

p – nanoparticle

c – empirical equation

REFERENCES

[1] C.S. Power, Technology Roadmap Concentrating Solar Power, Current. 5(2010) 1–52. doi:10.1787/9789264088139-en.

[2] G.C. Bakos, C. Tsechelidou, Solar aided power generation of a 300 MW lignite fired power plant combined with line-focus parabolic trough collectors field, Renew. Energy. 60 (2013) 1–8. doi:10.1016/j.renene.2013.05.024.

[3] M. Borunda, O.A. Jaramillo, R. Dorantes, A. Reyes, Organic Rankine Cycle coupling with a Parabolic Trough Solar Power Plant for cogeneration and industrial processes, Renew. Energy. 86 (2016) 651–663. doi:10.1016/j.renene.2015.08.041.

[4] I.K. Karathanassis, E. Papanicolaou, V. Belessiotis, G.C. Bergeles, Design and experimental evaluation of a parabolic-trough concentrating photovoltaic/thermal (CPVT) system with high-efficiency cooling, Renew. Energy. 101 (2017) 467–483. doi:10.1016/j.renene.2016.09.013.

[5] J. A. Clark, An analysis of the technical and economic performance of a parabolic trough concentrator for solar industrial process heat application, Int. J. Heat Mass Transf. 25 (1982) 1427–1438. doi:10.1016/0017-9310(82)90136-3.

[6] A. Thomas, H.M. Guven, Parabolic trough concentrators-design, construction and evaluation, Energy Convers. Manag. 34 (1993) 401–416. doi:10.1016/0196-8904(93)90090-W.

[7] S. Kalogirou, Parabolic Trough Collector System for Low Temperature Steam Generation: Design and Performance Characteristics, Appl. Energy. 55 (1996) 1–19. doi:10.1016/S0306-2619(96)00008-6.

[8] H. Price, E. Lüpfert, D. Kearney, E. Zarza, G. Cohen, R. Gee, R. Mahoney, Advances in Parabolic Trough Solar Power Technology, J. Sol. Energy Eng. 124 (2002) 109. doi:10.1115/1.1467922.

[9] Y. Xuan, Q. Li, Investigation on convective heat transfer and flow features of nanofluids, J. Heat Transfer. 125 (2003) 151. doi:10.1115/1.1532008.

[10] B. Sahin, G.G. Gultekin, E. Manay, S. Karagoz, Experimental investigation of heat transfer and pressure drop characteristics of Al2O3-water nanofluid, Exp. Therm. Fluid Sci. 50 (2013) 21–28. doi:10.1016/j.expthermflusci.2013.04.020.

[11] W.H. Azmi, K. V. Sharma, P.K. Sarma, R. Mamat, G. Najafi, Heat transfer and friction factor of water based TiO2 and SiO2 nanofluids under turbulent flow in a tube, Int. Commun. Heat Mass Transf. 59 (2014) 30–38. doi:10.1016/j.icheatmasstransfer.2014.10.007.

[12] W. Duangthongsuk, S. Wongwises, An experimental study on the heat transfer performance and pressure drop of TiO2-water nanofluids flowing under a turbulent flow regime, Int. J. Heat Mass Transf. 53 (2010) 334–344. doi:10.1016/j.ijheatmasstransfer.2009.09.024.

[13] A.A. Abbasian Arani, J. Amani, Experimental investigation of diameter effect on heat transfer performance and pressure drop of TiO2-water nanofluid, Exp. Therm. Fluid Sci. 44 (2013) 520–533. doi:10.1016/j.expthermflusci.2012.08.014.

[14] A.R. Sajadi, M.H. Kazemi, Investigation of turbulent convective heat transfer and pressure drop of TiO2/water nanofluid in circular tube, Int. Commun. Heat Mass Transf. 38 (2011) 1474–1478. doi:10.1016/j.icheatmasstransfer.2011.07.007.

[15] M.H. Kayhani, H. Soltanzadeh, M.M. Heyhat, M. Nazari, F. Kowsary, Experimental study of convective heat transfer and pressure drop of TiO 2/water nanofluid, Int. Commun. Heat Mass Transf. 39 (2012) 456–462. doi:10.1016/j.icheatmasstransfer.2012.01.004.

[16] H. Tyagi, P. Phelan, R. Prasher, Predicted Efficiency of a Low-Temperature Nanofluid-Based Direct Absorption Solar Collector, J. Sol. Energy Eng. 131 (2009) 41004. doi:10.1115/1.3197562.

[17] R. Saidur, T.C. Meng, Z. Said, M. Hasanuzzaman, A. Kamyar, Evaluation of the effect of nanofluid-based absorbers on direct solar collector, Int. J. Heat Mass Transf. 55 (2012) 5899–5907. doi:10.1016/j.ijheatmasstransfer.2012.05.087.

[18] R. a Taylor, P.E. Phelan, T.P. Otanicar, C. a Walker, M. Nguyen, S. Trimble, R. Prasher, Applicability of nanofluids in high flux solar collectors Applicability of nanofluids in high flux solar collectors, J. Renew. Sustain. Energy. 23104 (2011) 23104-1-0-15. doi:10.1063/1.3571565.

[19] T.P. Otanicar, P.E. Phelan, R.S. Prasher, G. Rosengarten, R.A. Taylor, Nanofluid-based direct absorption solar collector, J. Renew. Sustain. Energy. 2 (2010) 1–13. doi:10.1063/1.3429737.

[20] Y. He, Wang, Shufu, J. Ma ,F. Tian,Y. Ren, Experimental Study on the Light-Heat Conversion Characteristics of Nanofluids, Nanosci. Nanotech. Letters, 3, 4(2011),494-496. doi.org/10.1166/nnl.2011.1194.

[21] T. Yousefi, F. Veysi, E. Shojaeizadeh, S. Zinadini, An experimental investigation on the effect of Al2O3-H2O nanofluid on the efficiency of flat-plate solar collectors, Renew. Energy. 39 (2012) 293–298. doi:10.1016/j.renene.2011.08.056.

[22] O. Mahian, A. Kianifar, A.Z. Sahin, S. Wongwises, Performance analysis of a minichannel-based solar collector using different nanofluids, Energy Convers. Manag. 88 (2014) 129–138. doi:10.1016/j.enconman.2014.08.021.

[23] O. Mahian, A. Kianifar, S.Z. Heris, D. Wen, A.Z. Sahin, S. Wongwises, Nanofluids effects on the evaporation rate in a solar still equipped with a heat exchanger, Nano Energy. 36 (2017) 134–155. doi:10.1016/j.nanoen.2017.04.025.

[24] O. Mahian, A. Kianifar, S.A. Kalogirou, I. Pop, S. Wongwises, A review of the applications of nanofluids in solar energy, Int. J. Heat Mass Transf. 57 (2013) 582–594. doi:10.1016/j.ijheatmasstransfer.2012.10.037.

[25] P.K. Nagarajan, J. Subramani, S. Suyambazhahan, R. Sathyamurthy, Nanofluids for solar collector applications: A review, Energy Procedia. 61 (2014) 2416–2434. doi:10.1016/j.egypro.2014.12.017.

[26] N. Bozorgan, M. Shafahi, Performance evaluation of nanofluids in solar energy: a review of the recent literature, Micro Nano Syst. Lett. 3 (2015) 5. doi:10.1186/s40486-015-0014-2.

[27] T. Sokhansefat, A.B. Kasaeian, F. Kowsary, Heat transfer enhancement in parabolic trough collector tube using Al2O3/synthetic oil nanofluid, Renew. Sustain. Energy Rev. 33 (2014) 636–644. doi:10.1016/j.rser.2014.02.028.

[28] Y. Wang, J. Xu, Q. Liu, Y. Chen, H. Liu, Performance analysis of a parabolic trough solar collector using Al2O3/synthetic oil nanofluid, Appl. Therm. Eng. 107 (2016) 469–478. doi:10.1016/j.applthermaleng.2016.06.170.

[29] V. Khullar, H. Tyagi, P.E. Phelan, T.P. Otanicar, H. Singh, R.A. Taylor, Solar Energy Harvesting Using Nanofluids-Based Concentrating Solar Collector, J. Nanotechnol. Eng. Med. 3 (2013) 31003. doi:10.1115/1.4007387.

[30] A. Mwesigye, Z. Huan, J.P. Meyer, Thermodynamic optimisation of the performance of a parabolic trough receiver using synthetic oil-Al2O3 nanofluid, Appl. Energy. 156 (2015) 398–412. doi:10.1016/j.apenergy.2015.07.035.

[31] A. Kasaeian, S. Daviran, R.D. Azarian, A. Rashidi, Performance evaluation and nanofluid using capability study of a solar parabolic trough collector, Energy Convers. Manag. 89 (2015) 368–375. doi:10.1016/j.enconman.2014.09.056.

[32] E. Kaloudis, E. Papanicolaou, V. Belessiotis, Numerical simulations of a parabolic trough solar collector with nanofluid using a two-phase model, Renew. Energy. 97 (2016) 218–229. doi:10.1016/j.renene.2016.05.046.

[33] E. Bellos, C. Tzivanidis, K.A. Antonopoulos, G. Gkinis, Thermal enhancement of solar parabolic trough collectors by using nanofluids and converging-diverging absorber tube, Renew. Energy. 94 (2016) 213–222. doi:10.1016/j.renene.2016.03.062.

[34] S. Eiamsa-ard, K. Kiatkittipong, W. Jedsadaratanachai, Heat transfer enhancement of TiO2/water nanofluid in a heat exchanger tube equipped with overlapped dual twisted-tapes, Eng. Sci. Technol. an Int. J. 18 (2015) 336–350. doi:10.1016/j.jestch.2015.01.008.

[35] M.K. Abdolbaqi, R. Mamat, N.A.C. Sidik, W.H. Azmi, P. Selvakumar, Experimental investigation and development of new correlations for heat transfer enhancement and friction factor of BioGlycol/water based TiO2 nanofluids in flat tubes, Int. J. Heat Mass Transf. 108 (2017) 1026–1035. doi:10.1016/j.ijheatmasstransfer.2016.12.024.

[36] A. Menbari, A.A. Alemrajabi, A. Rezaei, Heat transfer analysis and the effect of CuO/Water nanofluid on direct absorption concentrating solar collector, Appl. Therm. Eng. 104 (2016) 176–183. doi:10.1016/j.applthermaleng.2016.05.064.

[37] Z. Uddin, S. Harmand, Natural convection heat transfer of nanofluids along a vertical plate embedded in porous medium, Nanoscale Res. Lett. 8 (2013) 64. doi:10.1186/1556-276X-8-64.

[38] S.Kalogirou, Solar energy engineering: process and systems. Copyright, 2009. doi:10.1016/B978-0-12-374501-9.00014-5.

[39] John A. Duffie, William A._Beckman. Solar Engineering of Thermal Processes. Copy right , 1980. John Wiley & Sons, 367.

[40] ASHRAE, Methods of testing to determine the thermal performance of solar collectors, ANSI/ASHRAE Stand. 93-2010. Am. Soc. Heating, Refrig. Air-Conditioning Eng. Inc. RA 2014 (2010). **(www.ashrae.org)**

[41] Y. Xuan, Q. Li, Heat transfer enhancement of nanofluids, Int. J. Heat Fluid Flow. 21 (2000) 58–64. doi:10.1016/S0142-727X(99)00067-3.

[42] H.C. Brinkman, The Viscosity of Concentrated Suspensions and Solutions, J. Chem. Phys. 20 (1952) 571–571. doi:10.1063/1.1700493.

[43] Y. Xuan, W. Roetzel, Conceptions for heat transfer correlation of nanofluids, 43 (2000) 3701–3707.

[44] B.C.Pak, Y.I.Cho, Hydrodynamic and heat transfer study of dispersed fluids with submicron metallic oxide particles., (1998) 151–170.

[45] R.A. Taylor, P.E. Phelan, T.P. Otanicar, R. Adrian, R. Prasher, Nanofluid optical property characterization: towards efficient direct absorption solar collectors, Nanoscale Res. Lett. 6 (2011) 225. doi:10.1186/1556-276X-6-225.

[46] O.A. Jaramillo, M. Borunda, K.M. Velazquez-Lucho, M. Robles, Parabolic trough solar collector for low enthalpy processes: An analysis of the efficiency enhancement by using twisted tape inserts, Renew. Energy. 93 (2016) 125–141. doi:10.1016/j.renene.2016.02.046.

[47] A.V. Arasu, T. Sornakumar, Performance Characteristics of Parabolic Trough Solar Collector System for, 7 (2006) 137–146.

[48] S.K. Das, S.U.S. Choi, W. Yu, T. Pradeep, Nanofluids: Science and Technology, 2007. doi:10.1002/9780470180693.

[49] Y.A. Çengel, A.J. Ghajar, Heat and Mass Transfer, 2011.Copy right 2015. New York: McGraw-Hill Publications.

[50] H.W. Coleman, W.G. Steele, Engineering application of experimental uncertainty analysis, AIAA J. 33 (1995) 1888–1896. doi:10.2514/3.12742.

[51] T. Yousefi, E. Shojaeizadeh, F. Veysi, S. Zinadini, An experimental investigation on the effect of pH variation of MWCNT–H2O nanofluid on the efficiency of a flat-plate solar collector, Sol. Energy. 86 (2012) 771–779. doi:10.1016/j.solener.2011.12.003.

574

575

576

577 Table 1. Various oxide nanoparticles with water as a base fluid in a circular pipe flow

Investigators **I.**	**Methods / Conditions**	**Nano particle / Base fluid/ particle size**	**Operating conditions** **II.**	**Remarks**
Sahin *et al.*[10]	Experimental / Turbulent	Al_2O_3/H_2O (ϕ= 0.5% to 4%)	Constant heat flux condition	Superior heat transfer was achieved for 0.5% volume concentration at Reynolds number of 8000.
Azmi *et al.*[11]	Experimental / Turbulent	TiO_2, SiO_2 /H_2O (ϕ= 0.5% to 3%)	Constant heat flux condition	Maximum heat transfer obtained was 26% for 1.0% of a TiO_2 nanofluid compared to a SiO_2 nanofluid, which exhibited 7% improvement in the same parametric conditions.
Duangthongsuk and Wongwises [12]	Experimental / Turbulent	TiO_2/H_2O (ϕ= 0.5% to 3%)	Constant heat flux condition	More than 0.1% volume concentration produced the highest heat transfer coefficient. (Numerically, 26% at 1.0% volume concentration).
Arani *et al.*[13]	Experimental / Turbulent	TiO_2/H_2O (ϕ= 0.01% to 0.02%)size of 10,20,30,50nm	Constant heat flux condition	20nm nanoparticle gives a maximum performance index when compared to other sizes of nanoparticles.
Sajadi and Kazemi [14]	Experimental / Turbulent	TiO_2/H_2O (ϕ= 0.05% to 0.25%)	Constant heat flux condition	The maximum convective heat transfer achieved was about 22% at ϕ= 0.25%.
Kayhani *et al.*[15]	Experimental / Turbulent	TiO_2/H_2O (ϕ= 0.1% to 2.0%)	Constant heat flux condition	The Nusselt number increased to8% at a vol. concentration of 2% with Re=11780

578

579

580

Table 2 Specifications of the parabolic trough solar collector

Specification	Dimensions
Parabolic trough collector length (L)	2.0 m
Parabola aperture length (W)	0.80 m
Focal distance (f)	0.24 m
Aperture Area (A_a)	1.6 m^2
Rim angle (ϕ_r)	80^o
Acceptance angle (θ)	0.4^o
Reflector thickness (approximately)	3mm
Concentration ratio (C)	15.6
Receiver tube inner tube diameter (d_i)	0.013 m
Receiver tube outer diameter (d_o)	0.016 m
Borosilicate glass inner diameter (d_{gi})	0.030 m
Borosilicate glass outer diameter (d_{go})	0.034 m

Fig.1. Photograph of the parabolic trough solar collector

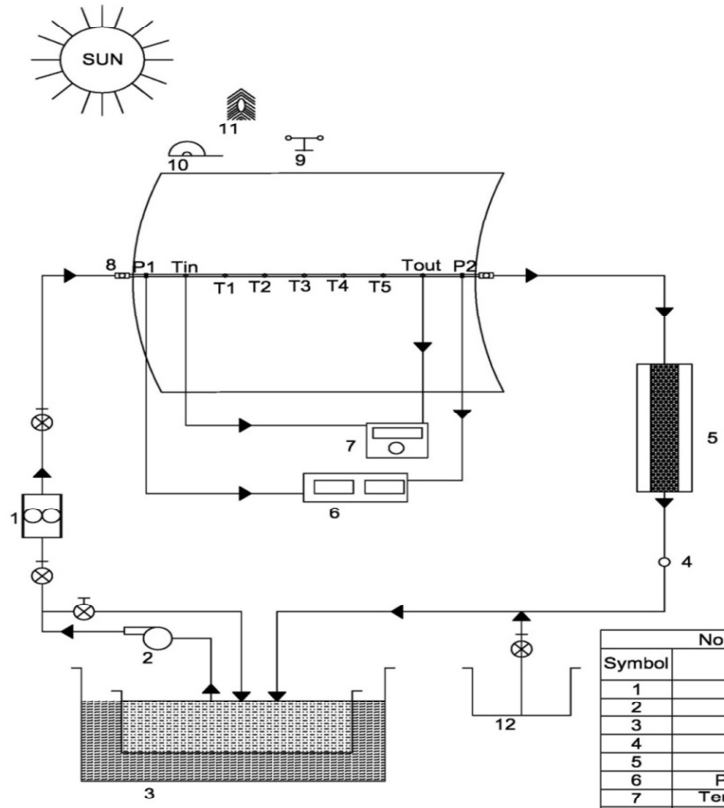

Nomenclature	
Symbol	Notation
1	Rotameter
2	Pump
3	Reservoir Tank
4	Sight Glass
5	Heat Exchanger
6	Pressure Indicator
7	Temperature Indicator
8	Mixer
9	Wind Velocity Sensor
10	Pyranometer
11	Ambient temperature Sensor
12	Make up fluid

Fig.2. Graphical layout of the experimental setup

Table 3 Stability of TiO_2 nanoparticles in water

S.No	Nanopowder	Particle concentration C (%)	Zeta potential ζ /mV	Stability activities	Stability time (days)
1		0.05	-23	Moderate stability	11
2	TiO_2	0.1	-28	Good stability	13
3		0.2	-45	Good stability	13

649
650
651
652
653
654
655
656
657
658
659

Table 4 Thermal conductivity and viscosity measurements

S.No	Nanopowder	Particle concentration C (%)	Thermal conductivity (W/mK)	% Enhancement in thermal conductivity[$]	Dynamic viscosity (cP)
1		0.05	0.61	1.66	0.92
2	TiO_2	0.1	0.66	9.24	1.02
3		0.2	0.68	13.21	1.26

660 [$]Base fluid thermal conductivity, k_{bf}=0.6 W/mK

661
662
663
664
665
666
667
668
669

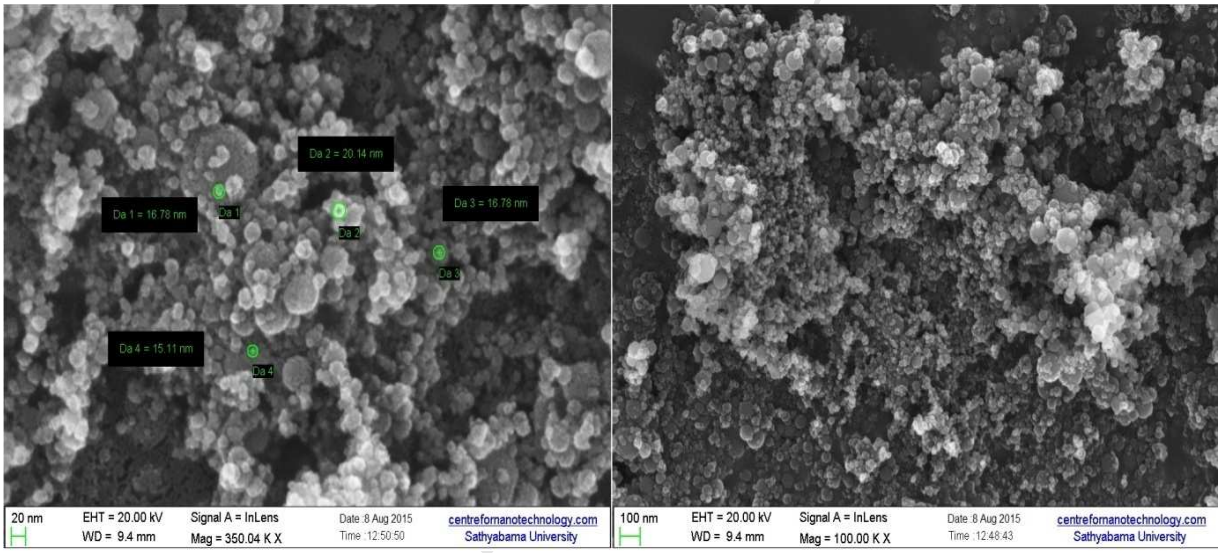

Fig.3. Scanning electron microscopy image of titanium nanoparticles

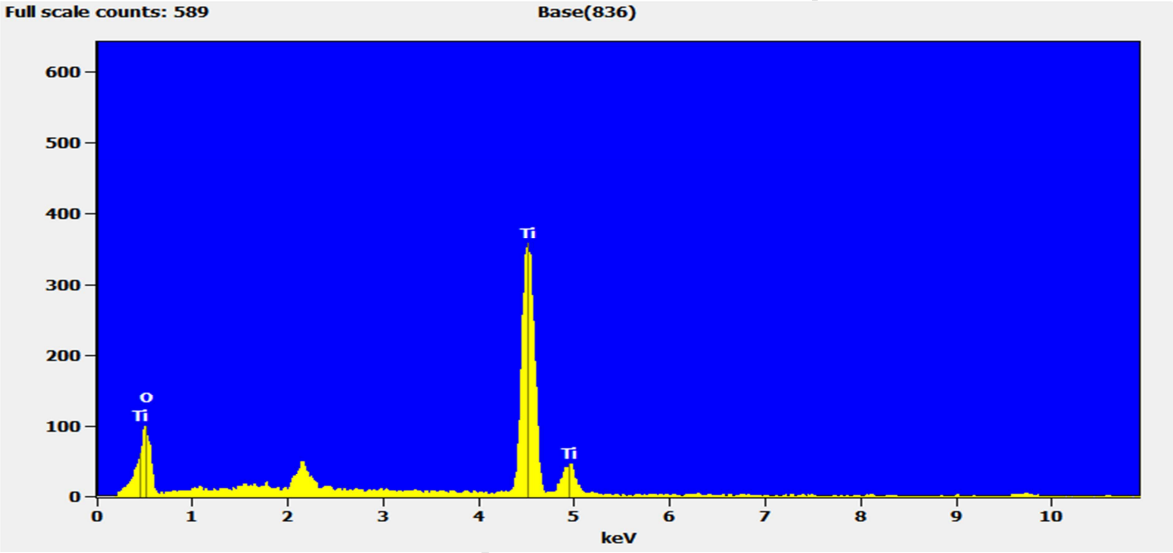

Fig.4. EDAX analysis of TiO_2 nanoparticles

706

707

708

709

710

711

712

713 Table 5 Theoretical equation for finding thermo-physical properties of TiO_2 nanofluids

714

Model name	Equations for models
Wasp model [41]	Eq. (1): Thermal conductivity (K_{nf}) $$K_{nf} = Kf\frac{Kp + 2kf - 2\alpha(Kf - Kp)}{Kp + 2kf + \alpha(Kf - Kp)}$$
Brinkman model [42]	Eq. (2): Viscosity (μ_{nf}) $$\frac{\mu_{nf}}{\mu f} = \frac{1}{(1-\varepsilon p)^{2.5}} = \frac{1}{(1-\phi^{2.5})}$$
Pak & Xuan model [43]	Eq. (3): Density (ρ_{nf}) $$\rho_{nf} = (1-\phi)\rho_{bf} + \phi\rho_p$$
Pak & Cho model [44]	Eq. (4): Specific heat (Cp_{nf}) $$Cp_{nf} = \frac{(1-\phi)\,\rho_{bf}\,Cp_{bf} + \phi\rho_p\,Cp_p}{\rho_{bf}}$$

715

716

717

718

719

720

721

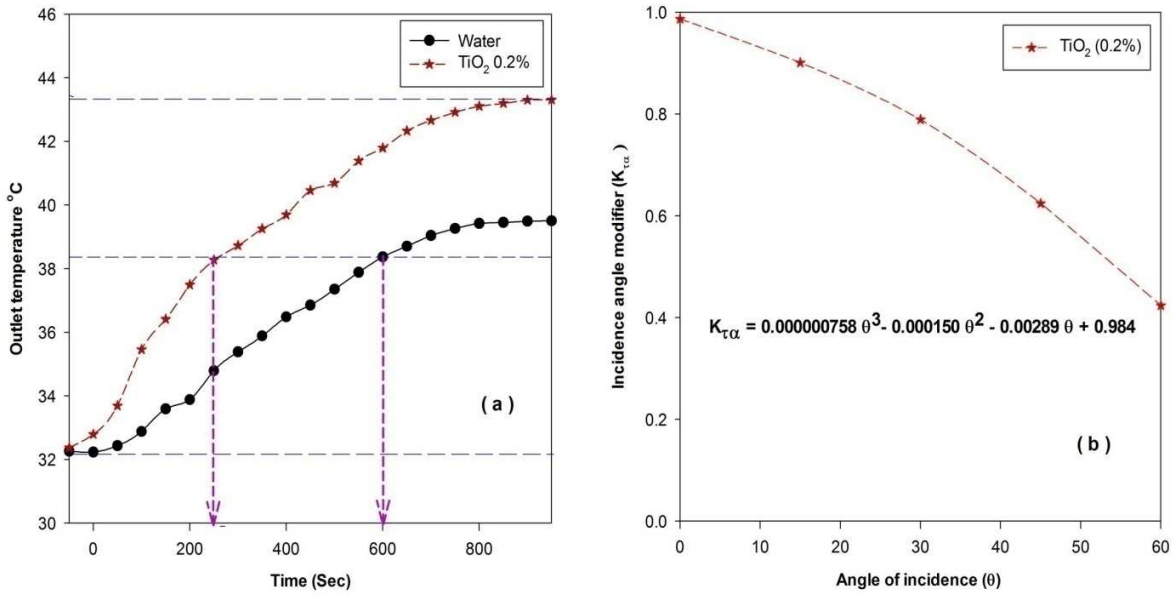

Fig.5. Variation in time, outlet temperature (a), and incidence angle with IAM (b)

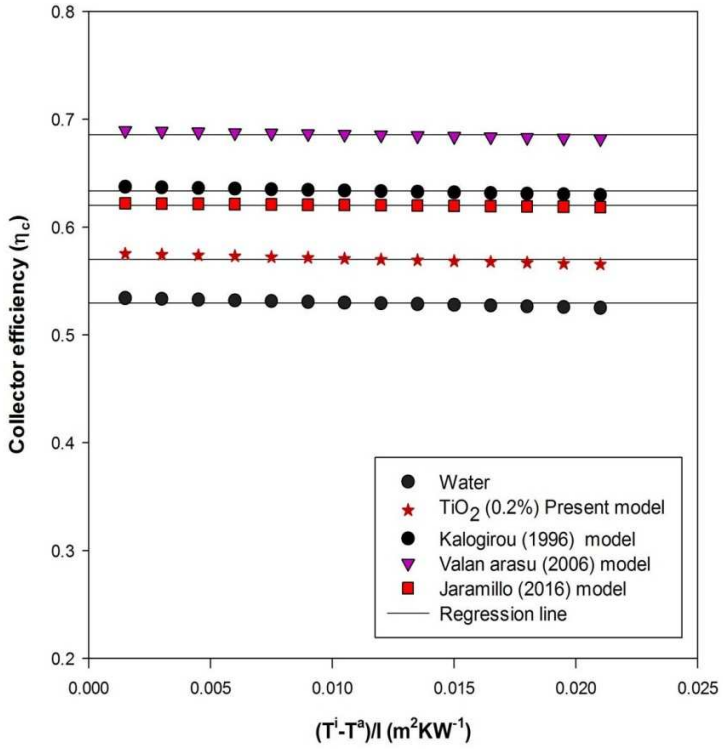

Fig. 6.Variation in the solar collector efficiency as a function of heat loss parameters

Table 6. Previous models and the present model equation for collector efficiency

Researchers	Efficiency equation
Present model – water (2017)	$\eta_c = 0.523 - 0.383*(T^i-T^a)/I$
Present model – TiO_2 (2017)	$\eta_c = 0.616 - 0.456*(T^i-T^a)/I$
Kalogirou model [7] (1996)	$\eta_c = 0.638 - 0.387*(T^i-T^a)/I$
Valan Arasu model [47] (2006)	$\eta_c = 0.690 - 0.387*(T^i-T^a)/I$
Jaramillo et al. model [46] (2016)	$\eta_c = 0.622 - 0.177*(T^i-T^a)/I$

Table 7. Various significant parameters for the present study

Study cases	Direct normalirradiance I (W/m^2)	Wind velocity (m/s)	Mass flow rate (kg/s)	T^i ^oK	T^o ^oK	Q_g (W)	Convective heat transfer (h) (W/m^2K)	Collector efficiency (η_c)
Case 1	872	2.31	0.017	304.64	315.76	707.22	616.12	50.65
Case 2	865	2.53	0.067	305.62	309.21	718.06	2087.65	51.95
Case 3	876	2.42	0.033	304.45	310.46	752.37	1310.75	53.68
Case 4	855	2.14	0.050	305.12	309.24	759.52	1928.16	55.49
Case 5	895	2.89	0.067	304.53	308.42	814.27	2702.69	56.86

Note: Cases 1 & 2- DI water, Cases 3-5-TiO_2 nanofluids ϕ=0.05%,0.1%,0.2% vol. concentration

791

792

793 Table 8 Equations for solar PTC heat transfer models and previous correlations

Specification	General equation	Input parameters
Reynolds number (Re)[48] as Eq.(10)	$Re = \left(\frac{\rho_{nf}\ u\ d_i}{\mu_{nf}}\right)$	u - velocity of fluid ρ_{nf}-Density of nanofluid μ_{nf}- Viscosity of nanofluid.
Convective heat transfer (h)[48] as Eq.(11)	$h_{nf} = \left(\frac{Q_g}{A_a\ (T^w - T^b)}\right)$	$Q_g = mC_{p_{nf}}(T^o - T^i)$ $T^w = \Sigma(T^{w1}+T^{w2}+T^{w3}+T^{w4}+T^{w5})/5$ $T^b = (T^i + T^o)/2$ T^b -Bulk mean temperature of the nanofluids T^w - Mean wall temperature of absorber tube
Nusselt number (Nu)[49] as Eq.(12)	$Nu = \left(\frac{h_{nf}\ d_i}{K_{nf}}\right)$	d_i- inner diameter of receiver tube k_{nf} is the thermal conductivity of the nanofluid h_{nf} - convective heat transfer coefficient for nanofluid
Friction factor (f)[49] as Eq.(13)	$f = \left(\frac{2\ \Delta P}{\rho_{nf}\ u^2(\frac{L}{di})}\right)$	ΔP - pressure drop of the solar PTC receiver tube. ρ_{nf}-Density of nanofluid L- length of the receiver tube
Performance Index (P_{index})[34]as Eq. (14)	$P_{index} = \left(\frac{h_{nf}}{h_{bf}}\right)$	h_{nf} - convective heat transfer coefficient for nanofluid h_{bf} - convective heat transfer coefficient for base fluid
Previous investigators	Previous correlations	
Mwesigye*et al.* [30]Eq. (15)	$Nu = 0.0104\ Re^{0.885} Pr^{0.374}$	
Pak and Cho [44]Eq. (16)	$Nu = 0.021\ Re^{0.8} Pr^{0.5}$	
Mwesigye *et al.* [30] as Eq.(17)	$f = 0.173\ Re^{-0.1974}$	
Petukhov's model [43]Eq.(18)	$f = (0.790\ ln\ Re - 1.64)^{-2}$	

794 $T^w$is the mean wall temperature of theabsorber tube, $T^b$is the bulk mean temperature of the

795 nanofluids, and thetemperature gradientis $\Delta T = (T^w - T^b)$

796
797
798
799
800
801
802
803
804

805 Table 9 Uncertainty values for instruments

Instruments	Range of instruments	Least count in measuring instrument	Uncertainty (%)
Thermocouple	0-200^{o}C	±1^{o}C	1.53%
Thermocouple (surface temperature)	0-300 ^{o}C	±1^{o}C	1.84%
Flow meter	0-10 lpm	±0.01lpm	1.63%
Pressure transducer	0-3.5bar	±0.01 bar	2.16%

806
807
808
809
810
811
812
813
814
815

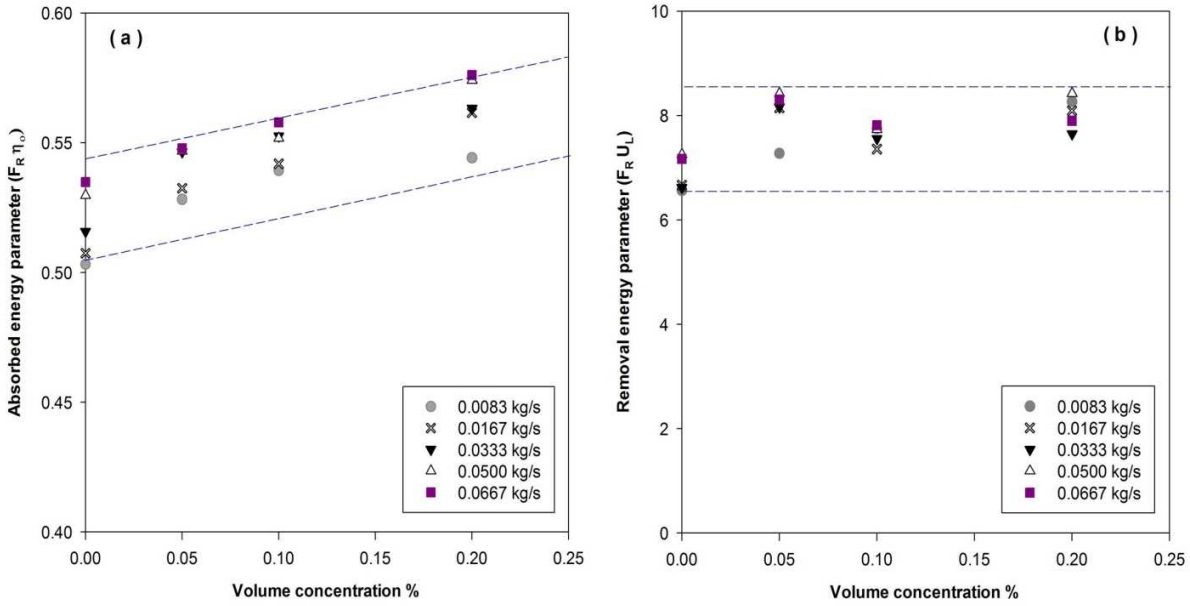

Fig. 7. Variation in the absorbed energy parameter (a) and removal energy parameter (b) with variations in volume concentrations at different flow rates

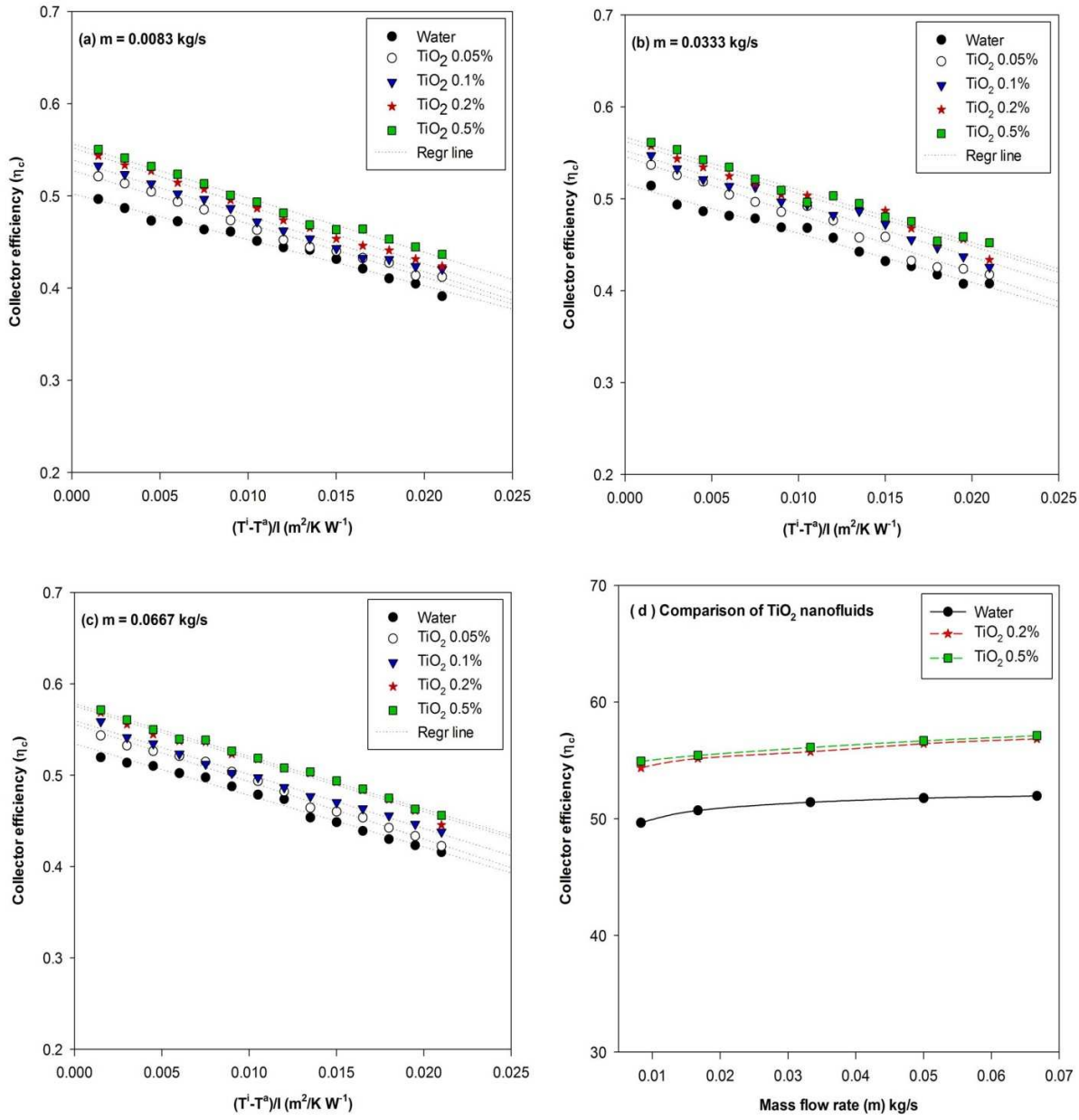

Fig.8. Effect of the heat loss parameter on collector efficiency for low (a), medium (b), and high (c) flow rates with variations in the volume concentrations, in addition to (d) collector efficiency comparison with various mass flow rates.

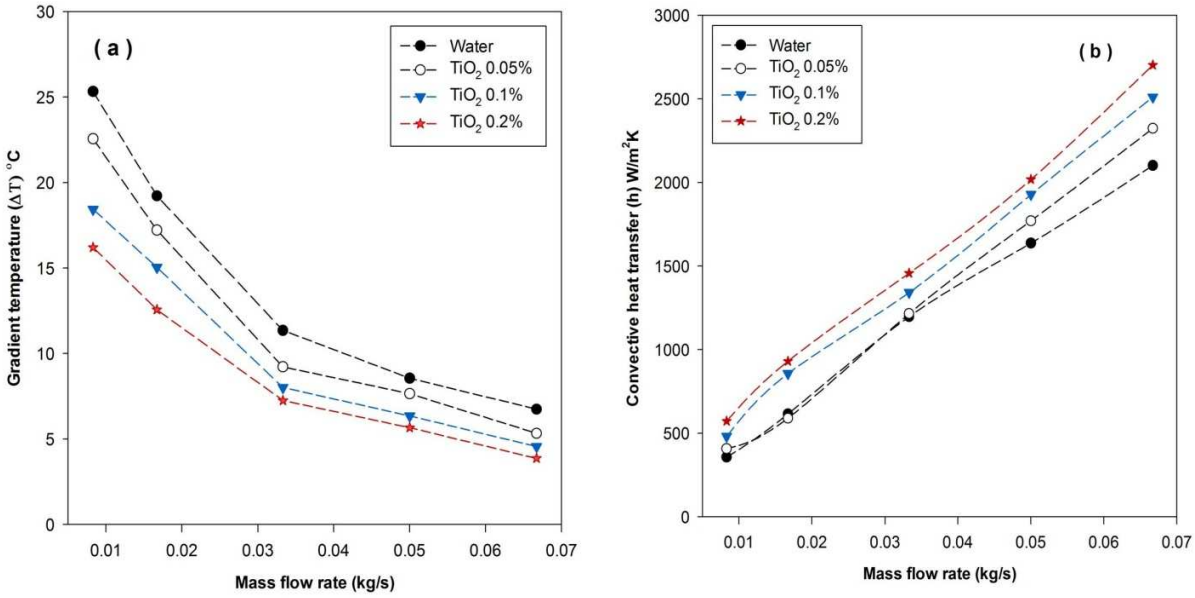

Fig.9. Comparison between temperature gradient (a) and the convective heat transfer coefficient (b) for various mass flow rates with different volume concentrations.

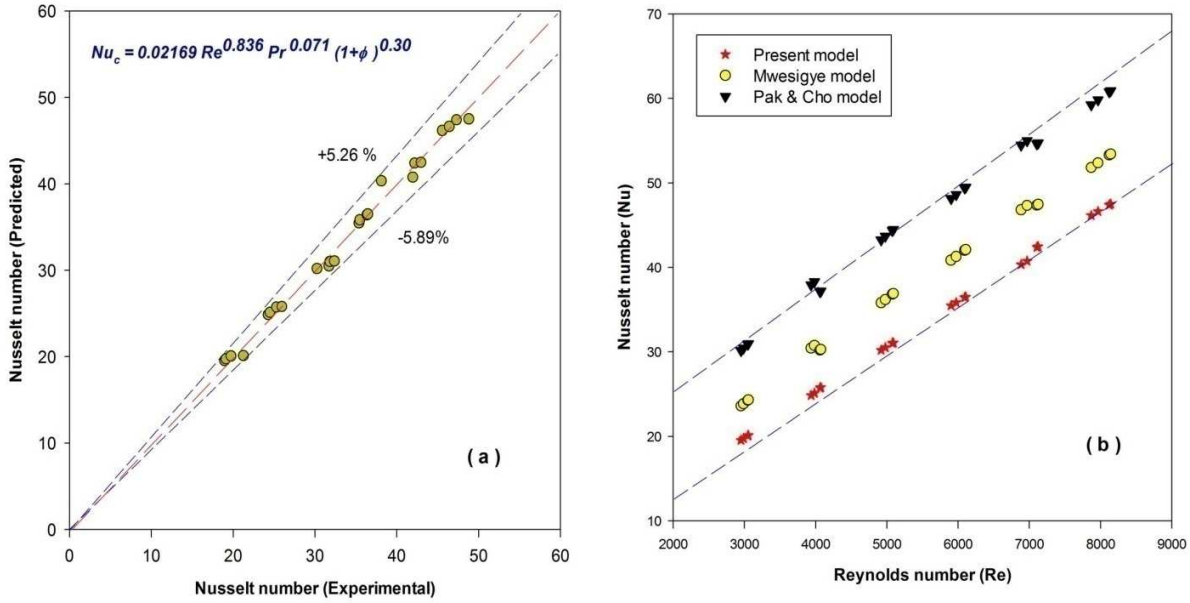

Fig.10 (a) Parity chart for the Nusselt number and (b)a validation of the present model with existing models.

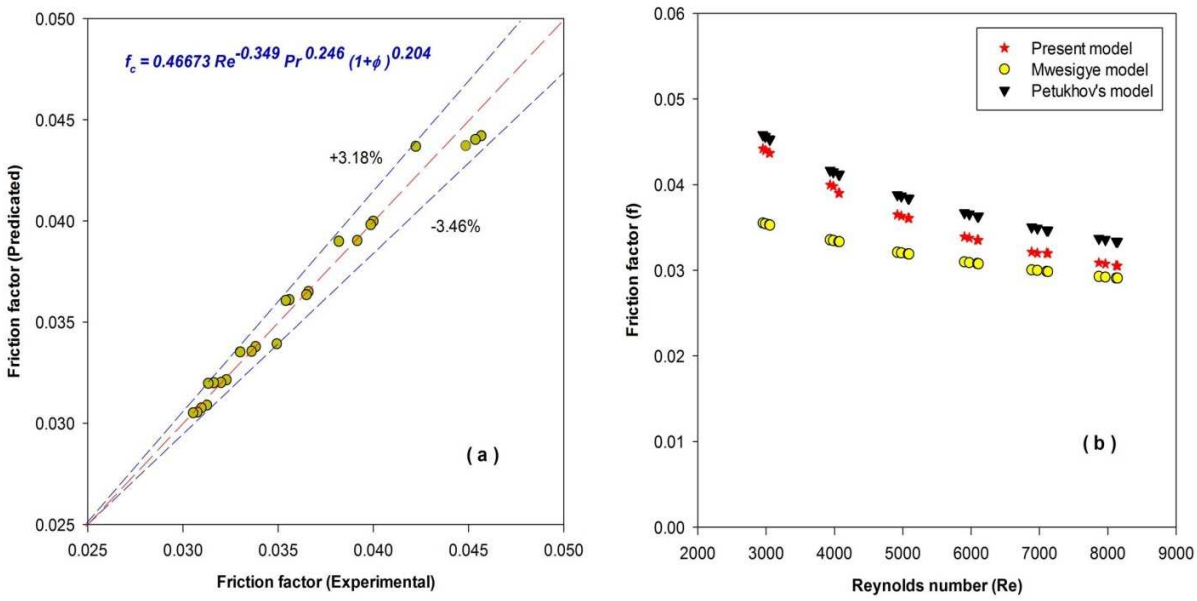

Fig.11(a) Parity chart for the friction factor and (b) validation of the solar PTC model with previous models.

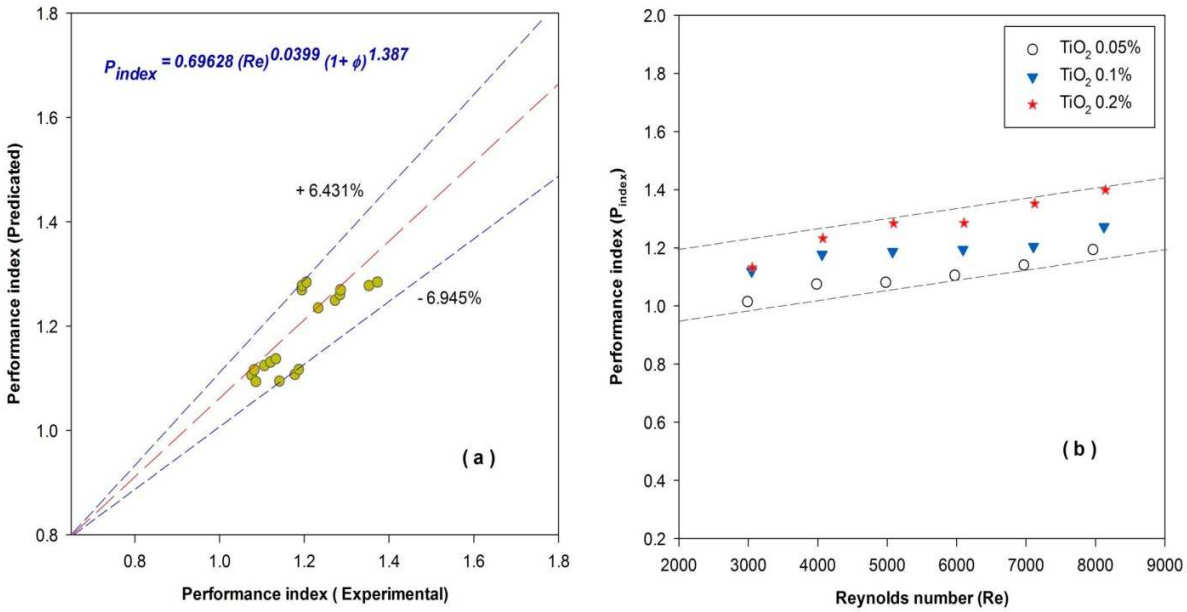

Fig.12(a) Parity chart for performance index and (b)effects of the Reynolds number on the performance index of a solar PTC at various volume concentrations.

HIGHLIGHTS:

- Experiments were carried out on a parabolic trough collector using TiO_2 nanofluids.
- Tests were performed for volume concentrations up to 0.2% under turbulent flow.
- Collector efficiency can be enhanced using nanofluids up to 8.66% compared to water.
- Heat transfer coefficient raised about 23% by replacing nanofluid instead of water.